Marine Biology (2026) 173:34
https://doi.org/10.1007/s00227-025-04792-4

ORIGINAL PAPER

Bomb radiocarbon reveals keratin growth dynamics in loggerhead (*Caretta caretta*) and green (*Chelonia mydas*) turtles

Bethan Linscott[1,2] · Amy A. Wallace[1,3] · Lorena Becerra-Valdivia[4] · Matt R. P. Harris[5] · Alexandra L. Fireman[1] · Jenna D. Bennett[1] · William F. Patterson III[6] · Hannah B. Vander Zanden[1]

Received: 18 July 2025 / Accepted: 29 December 2025 / Published online: 28 January 2026

Abstract

Incrementally formed biological tissues can serve as archives of biochemical information pertaining to the life histories of organisms. The sequential isotopic analysis of marine turtle scute keratin is increasingly used for ecological reconstruction, but the timescales represented by these tissues remain poorly understood. Here, we present a method to establish scute growth rates using sequential radiocarbon (^{14}C) measurements on samples taken from loggerhead (*Caretta caretta*) and green turtles (*Chelonia mydas*) stranded along the Florida coast. Using a $\Delta^{14}C$ coral-otolith reference series and a Bayesian modelling approach, we reconstructed the rate of keratin formation in 24 individuals (representing 120 radiocarbon measurements) and detected synchronous declines in scute growth rates that may be linked to marine environmental stress. Our results provide a chronological framework for the ecological interpretation of biogeochemical data from green and loggerhead turtle scutes and demonstrate the potential for ^{14}C analysis to investigate the growth dynamics of other incremental tissues.

Keywords Sea turtle · Scute · Radiocarbon · Gulf of Mexico · Atlantic

Introduction

Accretionary tissues such as hair, nails, tooth enamel, eye lenses and otoliths provide valuable chronological records for life history reconstructions (Cerling et al. 2009; Trueman et al. 2013; Wallace et al. 2014; Linscott et al. 2023). Because these tissues grow incrementally, they incorporate biochemical signals that can reflect dietary, physiological, and environmental conditions at the time of formation (Katzenberg and Waters-Rist 2018; Doubleday et al. 2025). These tissues permit data collection at multiple chronological points from a single sample, enabling the high-resolution reconstruction of biological and environmental changes. In particular, the analysis of accretionary tissues is valuable in reconstructing the life histories of elusive marine species such as marine turtles that are otherwise difficult to observe directly (Haywood et al. 2019). However, knowledge of the formation rates of accretionary tissues is critical to accurate interpretation of biochemical data.

Sea turtles are long-lived, late maturing marine reptiles with complex life cycles. All six species of marine turtles found in U.S. waters, including the loggerhead turtle (*Caretta caretta*) and green turtle (*Chelonia mydas*) are

Responsible Editor: P. Casale.

Bethan Linscott and Amy A. Wallace are joint first authors.

✉ Bethan Linscott
bethanlinscott@earth.miami.edu

✉ Amy A. Wallace
amy.wallace@oregonstate.edu

1 Archie Carr Center for Sea Turtle Research, Department of Biology, University of Florida, Gainesville, FL 32611, USA

2 Robert K. Johnson Center for Marine Conservation, Rosenstiel School of Marine, Atmospheric and Earth Science, University of Miami, Miami, FL 33149, USA

3 Cooperative Institute for Marine Ecosystem and Resources Studies, Hatfield Marine Science Center, Oregon State University, Newport, OR 97365, USA

4 Department of Anthropology and Archaeology, University of Bristol, Bristol BS8 1TH, UK

5 National Isotope Centre, Earth Sciences New Zealand, Lower Hutt 5010, New Zealand

6 Fisheries and Aquatic Sciences, University of Florida, Gainesville, FL 32611, USA

listed and protected under the U.S. Endangered Species Act of 1973 (Seminoff et al. 2015; Bolten et al. 2019). Understanding their spatial distribution, movement patterns, and diets is critical for the development of effective conservation and management strategies, particularly in a rapidly changing climate (Ehrlén and Morris 2015). Stable isotope analysis of carbon ($\delta^{13}C$) and nitrogen ($\delta^{15}N$) has emerged as a powerful tool for reconstructing sea turtle ecology and is now widely applied across all seven species (Pearson et al. 2017; Figgener et al. 2019; Haywood et al. 2019; Seminoff and Phillott 2020). In particular, sequential $\delta^{13}C$ and $\delta^{15}N$ analysis of scutes—the hard, inert keratinous plates that cover the bony carapace (shell) of all marine turtles except the leatherback (*Dermochelys coriacea*)—has become increasingly valuable for investigating life history, migration, feeding ecology, and trophic dynamics (Reich et al. 2007; Vander Zanden et al. 2010, 2013; López-Castro et al. 2014; Shimada et al. 2014; Van Houtan et al. 2023; Fireman et al. 2024). For example, fluctuations in $\delta^{13}C$ and $\delta^{15}N$ values among increments of a single scute biopsy can reflect ontogenetic shifts in habitat and diet that would otherwise be undetectable in non-accretionary tissues with high turnover rates such as plasma or red blood cells (Reich et al. 2007).

Since scute keratin accumulates continuously from the basal epidermis (with the oldest tissue at the outermost surface (Vander Zanden et al. 2010) and remains inert after formation, it retains a chronological sequence of biochemical information that can be used to reconstruct an individual's life history. For example, Reich et al. (2007) detected the elusive ontogenetic habitat shift of juvenile green turtles from oceanic to neritic environments using sequential $\delta^{13}C$ and $\delta^{15}N$ analysis of scutes, solving a long-standing mystery surrounding the 'lost years' of Atlantic green turtles. However, without knowledge of scute keratin growth rates, the timescale represented by sequential scute isotope data remains uncertain. Establishing the temporal resolution of these isotopic records is critical for conservation and management efforts, since the timing and pace of ontogenetic shifts, habitat use and exposure to ecological stressors can directly impact survival. Chronologically-resolved scute records can help to non-invasively identify when sea turtles occupy high-risk habitats and better link life-stage–specific threats to individual histories. Existing estimates of scute growth rates in sea turtles are based on the observed rate of carbon turnover in juvenile turtles, scaled to adult body size, and applied to an observed isotopic shift in adults (Reich et al. 2008; Vander Zanden et al. 2010). This approach suggests growth rates of 0.6 y per 50 µm of keratin in loggerheads (Vander Zanden et al. 2010), and 0.41 y per 50 µm of keratin in adult green turtles (Vander Zanden et al. 2013). However, the outermost (oldest) scute layers are susceptible to mechanical wear over time (Reich et al. 2007), so a cross section of a scute biopsy does not necessarily represent the full lifetime of an individual, except possibly in some juveniles.

Radiocarbon (^{14}C) dating is a method primarily used in archaeology and Quaternary science to establish the age of carbon-containing materials and compounds. It relies on the predictable radioactive decay of ^{14}C into ^{14}N via beta emission within a closed system. Radioactive carbon is generated in the upper atmosphere and is incorporated into the biosphere via photosynthesis, and into the hydrosphere via diffusion. Living organisms maintain radioactive carbon equilibrium with their surroundings through the diet, but upon death, cease to obtain new ^{14}C (Hajdas 2008).

Because atmospheric ^{14}C production has fluctuated over time, radiocarbon ages must be calibrated against known-age samples to obtain meaningful calendar age estimates. In the terrestrial environment, this calibration is primarily achieved by comparing the radiocarbon measurement of dendrochronologically-dated tree rings to that of the sample (Bronk Ramsey 2008a). In the marine environment, calibration is complicated by geographically varying timescales for CO_2 exchange between the atmosphere, surface waters and deep ocean (Bronk Ramsey 2008a), and as such, radiocarbon dating has largely been used as a tool to reveal ocean circulation patterns (for example, see Druffel and Griffin (1993).

Nuclear weapons testing in the mid-20th century almost doubled the ^{14}C concentration in the atmosphere (Bronk Ramsey 2008b), until the Limited Test Ban Treaty of 1963 drastically reduced nuclear testing (Hajdas et al. 2021). This rapid, anthropogenically-driven increase in atmospheric ^{14}C was followed by a gradual decline as ^{14}C was absorbed by the terrestrial and marine biospheres. The resulting 'bomb pulse' is a useful environmental tracer due to differences in the rates of exchange between different carbon reservoirs. In the marine environment, bomb ^{14}C is frequently used as a chronometer for age validation (Kalish 1993; Kastelle et al. 2008; Barnett et al. 2020; Chamberlin et al. 2023) or even direct age estimation of bony fishes (Andrews et al. 2011) through the ^{14}C dating of sequentially formed otoliths. It has also been used in the age validation of hawksbill turtle (*Eretmochelys imbricata*) scute layers (Van Houtan et al. 2016). Since the bomb pulse is recorded in the known-age growth rings of corals globally (with an offset resulting from the degree of ^{14}C mixing in the local marine environment), ^{14}C measurements obtained for specimens of unknown age can be calibrated against local coral curves to determine an accurate calendar age. The bomb pulse is well documented in hermatypic corals of the Gulf of Mexico and northern Caribbean Sea (Druffel and Linick 1978; Druffel 1980; Wagner 2009), making this an ideal location to develop a

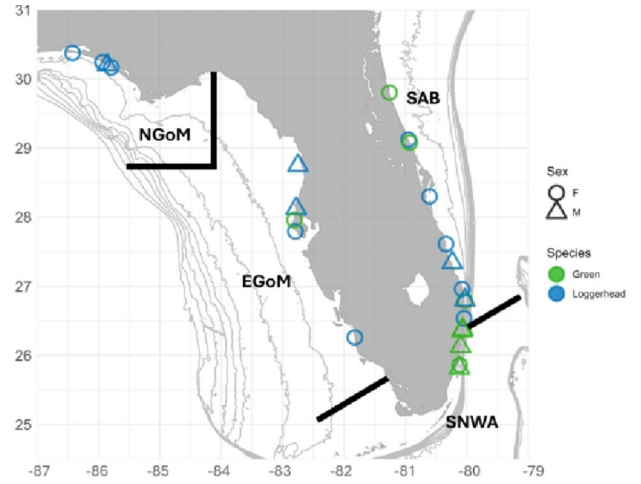

Fig. 1 Map of the Florida stranding locations of successfully dated green ($n = 9$) and loggerhead ($n = 15$) sea turtles sampled in this study. All individuals stranded in one of four general regions along the coast of Florida identical to those outlined in Vander Zanden et al. (2015). NGoM = Northern Gulf of Mexico, EGoM = Eastern Gulf of Mexico, SNWA = Subtropical Northwest Atlantic, SAB = South Atlantic Bight

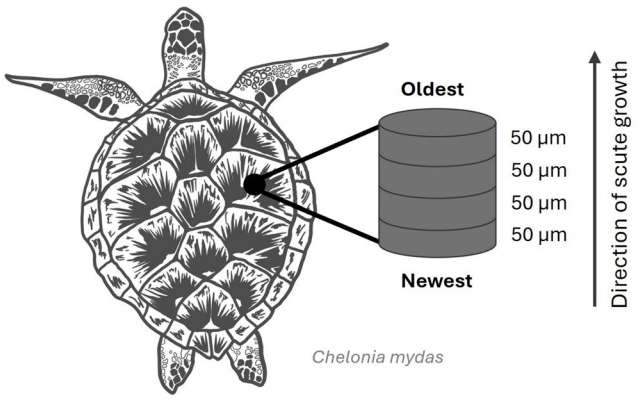

Fig. 2 Schematic showing the scute sampling location (2nd lateral scute) for green turtles. Note that the 3rd lateral scute was selected for loggerhead turtles

local marine ^{14}C calibration curve with which to determine loggerhead and green sea turtle scute growth rates.

Here, we characterize loggerhead and green turtle scute growth rates through sequential ^{14}C dating of scute biopsies taken from 24 individuals that stranded in the Gulf of Mexico and along the east coast of Florida. We use a Bayesian chronological modelling approach to determine scute growth rate variability within and among individuals, detecting synchronous and geographically widespread declines in keratin accumulation rates. Our results offer new growth rate estimates for interpreting scute isotopic records—which represent the longest non-invasive chronological archive available from live turtles—and demonstrate the method's potential for reconstructing growth in other incrementally formed tissues.

Materials and methods

Sampling

Scute samples were obtained from 15 stranded and deceased loggerhead turtles and 17 stranded and deceased green turtles with varying straight carapace lengths (SCL) from a combination of Sea Turtle Stranding and Salvage Network (STSSN) necropsy sessions and from rehabilitation facilities where patients died on site. The stranding date is used as the estimated date of death for all individuals. All individuals stranded in one of four general regions along the coast of Florida identical to those outlined in Vander Zanden et al. (2015) (Fig. 1). Three of the green turtles (Turtles 13588, 13590 and 13776) were juveniles and likely belong to the oceanic life stage; a period when juveniles occupy open ocean environments for several years during development (Bolten 2003). All other individuals in this study are of a size consistent with the neritic life stage, when foraging primarily occurs in benthic environments close to the shore (Bolten 2003). For green and loggerhead turtles, the central region of the second and third lateral scutes were selected for sampling, respectively (Fig. 2). This area is the thickest part of the scute and should therefore provide the longest isotopic record (López-Castro et al. 2014).

All metal tools and aluminum foil used to sample, store, and prepare samples were baked in a muffle furnace at 450 °C for four hours prior to use to ensure all organics were removed. Glassware was acid-washed and baked in a muffle furnace at 450 °C prior to use. During necropsy sessions, scutes were removed from carapaces using stainless-steel knives and stored in baked aluminum foil within Ziplock bags at −20 °C. Prior to processing, the scutes were removed from the freezer and cleaned of surface debris such as dirt and algal growth using a baked stainless-steel scoopula and ultra-pure water (18.2 MΩ cm^{-1}). A 6-mm diameter keratin biopsy (Fig. 2) was removed from the central region of each scute using a reusable stainless steel biopsy punch, which was baked at 450 °C between each sample. Each scute biopsy was then soaked in ultra-pure water for at least 12 h to remove any remaining dirt and debris, and subsequently dried for 24 h in a drying oven at 60 °C.

Each keratin biopsy sample was affixed dorsal-side up (to expose the oldest tissue) to a microscope slide using Crystal Bond™ adhesive resin. Layers of keratin were removed in 50 µm increments (Fig. 2) using a Sherline 5100 A-DRO benchtop mill equipped with a 1/16th drill bit rotating at speeds between 55 and 75 RPM. The drill bit was baked at 450 °C between keratin biopsies. The resulting powder was inspected under a dissecting microscope for residual resin. Milling was terminated once a removed layer contained resin fragments, and this layer was excluded from analysis.

Consequently, the most recent layer of scute was not sampled for any turtle. All samples were sent to the National Ocean Sciences Accelerator Mass Spectrometry facility (NOSAMS) for ^{14}C analysis using a MICADAS system (Ionplus AG, Switzerland). Reported precision is 3–4‰.

The Crystal Bond™ resin used to affix the scute samples to glass slides for sub-sampling presented a potential source of ^{14}C-depleted petrocarbon contamination. Whole biopsies and scute layers that returned pre-modern ages ($\Delta^{14}C$ value of less than 0‰) were excluded from further analysis. Of the 17 green turtle scute biopsies, eight returned entirely pre-modern $\Delta^{14}C$ values and were likely to be contaminated by the adhesive. These eight individuals are therefore excluded from further analysis. All the loggerhead scute biopsies returned entirely modern $\Delta^{14}C$ values except for one individual (Turtle 13326), which exhibited contamination of the two keratin layers closest to the adhesive resin. The contaminated layers from that individual were therefore excluded from further analysis. In total, the number of individuals retained for further analysis was nine green and 15 loggerhead turtles. The inconsistency in the proportion of contaminated green and loggerhead biopsies from turtles may be due to slight differences in scute thickness between species – green turtles tended to have thinner scute biopsies than loggerheads on average, which may have allowed excess adhesive to exude up from the ventral surface and up the sides of the biopsy, contaminating more layers proportionally.

^{14}C calibration

We generated a ^{14}C calibration curve for the Gulf of Mexico and northern Caribbean Sea using ^{14}C data from known-age hermatypic corals (Druffel and Linick 1978; Druffel 1980, 1989; Wagner 2009; Wagner et al. 2009; Moyer and Grottoli 2011) and known-age red snapper otoliths (Barnett et al. 2018; Chamberlin et al. 2023) spanning the period from 1944 to the present day (https://doi.org/10.7266/5vsz0kfh, Fig. S1; Table S1). For years with multiple independent measurements, we calculated a weighted average based on the measurement uncertainty. In cases where measurement uncertainties were not published, we used the mean measurement uncertainty reported by the laboratory at which those measurements were made. We imported these data into OxCal v.4.4.4 (Bronk Ramsey 2009a) and used this calibration curve to produce Bayesian models for all but one of the of the turtles (Turtle 13776). For this juvenile green turtle in the oceanic life stage (see Discussion), we constructed a model using the atmospheric bomb-pulse calibration curve Bomb21NH2 (Hua et al. 2021) for use with OxCal v.4.4.4 (Bronk Ramsey 2009a).

Scute growth rates

We produced Bayesian chronological models for each of the scute biopsies using OxCal v4.4.4 (Bronk Ramsey 2009a) and the coral-otolith reference series. Because scute keratin forms incrementally, prior knowledge about the order of the scute layers can be used to produce refined probability density functions (PDFs) for each ^{14}C measurement using a Markov Chain Monte Carlo simulation approach (Bronk Ramsey 2008b). The result is a refined sequence of model-predicted dates for each scute biopsy that incorporates measurement uncertainty, calibration uncertainty, and the incremental relationship between each 50 µm layer of keratin.

The rate and intra-individual variability of marine turtle keratin formation is unknown. Therefore, we built Poisson depositional models (*P_Sequence)* with variable *k* values (rate of accumulation events per unit depth) for each scute biopsy to allow for variation in keratin deposition through time (see Bronk Ramsey (2008b) for mathematical formulation). These models used a *k* value (k_0) of 0.01, an interpolation rate of 0.005 (producing outputs every 2 µm), and a log_10 (k/k_0) of U(−2,2), permitting *k* to vary by two orders of magnitude in either direction. The upper boundary for each model corresponds to the stranding date of each turtle in fractional years. The model interpolates between dated layers and evaluates a biologically realistic range of deposition scenarios (*k* values), identifying those that best fit the data. Since there are multiple factors that may affect the ^{14}C concentration in the scute layers—such as dietary carbon input from organisms with inbuilt age, e.g. long-lived sponges and corals, or those that incorporate dietary carbon from ocean upwelling and oil seeps, as well as contamination—we assigned each measurement a 5% prior probability of being an outlier within an r-type Outlier Model (Bronk Ramsey 2009b). Measurements are progressively down-weighted by the model as their posterior outlier probability increases. Keratin growth rates were calculated based on the temporal intervals between the predicted age estimates. These model-derived accumulation rates were then used to estimate the mean scute growth rate for each turtle (see Supporting Information: *OxCal code (CQL) for Bayesian chronological models* for CQL code).

Welch's t-tests ($\alpha = 0.05$) were performed to compare mean scute growth rates across species, sex, and life stage. To investigate differences in scute growth rate variability between green and loggerhead turtles, we calculated the coefficient of variation for each individual and performed a Welch's t-test ($\alpha = 0.05$). To compare the relative variability in scute growth rates between green turtles and loggerheads, we calculated the coefficient of variation (CV) for

each individual based on the time series data of annual scute growth rates.

Changepoint analysis of model-predicted scute growth rates

To empirically identify instances of significant change in the scute records, we applied changepoint analysis to the growth rates, incorporating age uncertainty by analyzing changes across ensemble members from the Bayesian age model for each turtle. We utilized the MCCPT R package (Cadd et al. 2021), an adaptation of the Killick and Eckley (2014) implementation of changepoint analysis in R. We generated PDFs using unweighted Gaussian kernel density estimation for changepoints in accumulation rates identified across the 2000 age model iterations generated by OxCal for each turtle.

OxCal-derived age model ensemble members for each turtle were first interpolated using a monotonic cubic spline approach to a resolution of 1 µm, to provide a consistent depth resolution (Fig. S35). Because the scute growth rates of most individuals change continuously, individual turtle scute growth rates were converted to discrete gradients (Fig. S36). Gradient values were rescaled to values between 0 and 100 to allow for shifts in means to be detected without the presence of negative values. We used the binned segment method to identify shifts in the mean interpolated turtle scute growth rates, specifying a number of segments equal to the number of radiocarbon dates for each turtle in order. We iteratively specified increasing numbers of changepoints for each record until all major observed changes were captured—that is, there were no overlapping segments in the identification of changes in the mean gradient.

By summing the PDFs associated with positive (increasing) and negative (decreasing) changes in turtle growth rates across all the age model ensemble members, we identified years of increased change probability across the analyzed turtle population, which appear as pronounced peaks in the summed PDF distribution. We categorized the types of changes within the 'increasing' and 'decreasing' categories as follows: (a) accelerating or stabilizing, in which the slope becomes more or less steep (e.g., a turtle with an already decreasing scute growth rate undergoes an even steeper decline in growth rate, and vice versa); (b) a reversal, in which the change entails a shift between stable, increasing, or decreasing rates in adjacent segments; and (c) a complete reversal, in which the change is from increasing to decreasing and vice versa.

To accomplish the classification, linear regressions were fit to the growth rate values for each growth rate segment (between changepoints; Supporting Information Fig. S37, Table S2). Changes in the slope of the regressions across each changepoint (i.e., between segments) were then calculated. To account for differing total growth rates between turtles, rate changes across changepoints were normalized (Eq. 1) by the total growth rate range of each turtle, expressed as a percentage. Rate units are given in µm/year:

$$slope' = \frac{slope}{\max(growth\ rate) - \min(growth\ rate)} \times 100 \quad (1)$$

Normalization ensures that once the thresholds outlined below are applied, the final PDFs are not overrepresented by turtles that grow faster overall.

To identify periods of 'stable' growth rates (as opposed to increasing and decreasing), we applied a normalized slope threshold of +/− 10 µm/year/year. Segments lying within this normalized slope range are classed as 'stable', with the scute keratin growing at a near-consistent rate during the time encompassed by the segment. We classed major changes as those with a change in normalized slope of >25%.

Results

Sequential $\Delta^{14}C$ analysis

We obtained 77 sequential radiocarbon measurements for 15 sub-adult and adult loggerheads with SCLs between 69 and 103 cm. One individual (Turtle 13326) exhibited pre-modern radiocarbon ages in the two deepest keratin layers and were assumed to be contaminated by the adhesive used to affix the scute biopsies to microscope slides. The radiocarbon data for those layers were therefore excluded from further analysis. The $\Delta^{14}C$ values of successive loggerhead keratin layers generally decreased relative to scute depth as expected when compared to the coral-otolith reference series (Supporting Information, Figs. S1, S2). Three of the female loggerhead turtles (Turtles 13324, 13587 and 13764), however, exhibited $\Delta^{14}C$ values lower than any of the known-age corals or otoliths that comprise the calibration curve (<18‰). These samples were therefore excluded from subsequent Bayesian chronological modelling because they cannot be reliably calibrated (see Discussion), but data are available in GRIID-C (https://data.griidc.org/data/F3.x304.000:0004).

We obtained 77 sequential radiocarbon measurements for 17 juvenile, sub-adult and adult green turtles with SCLs between 24 and 91 cm. Of those 17, the biopsies of eight individuals returned pre-modern radiocarbon ages and were assumed to be contaminated with the adhesive used to affix the scute to the slides. These eight individuals were

therefore excluded from subsequent Bayesian chronological modelling, but data are available in GRIID-C (https://data.griidc.org/data/F3.x304.000:0004). Of the remaining nine, three individuals represent the juvenile open ocean 'oceanic' life stage (Turtles 13588, 13769 and 13776) whilst the rest likely reflect the neritic life stage based on straight carapace length (Bolten et al. 2003). Green turtle keratin $\Delta^{14}C$ values generally decreased with scute depth, as expected (Supporting Information, Fig. S3), but there were instances of one or more scute layers deviating from the expected monotonic age-depth relationship in all nine individuals.

Scute growth rates

Bayesian chronological modelling using the coral-otolith reference series resolved all instances where individual scute layers deviated from the expected monotonic $\Delta^{14}C$-depth relationship through the incorporation of stratigraphic priors, providing insights into scute growth rate variability within individuals over time (Figs. S4-S27). In the loggerheads, based on model-predicted accumulation rates (Fig. 3; Table 1; excluding specimens in italics which could not be reliably modelled; see Discussion), the mean time (±1 SD) required for the growth of 50 µm of scute keratin was 0.79±0.53 y (n=11). Intra-individual variation in scute growth rates through time was apparent in all individuals, with nine individuals exhibiting decreasing rates and three exhibiting increasing rates. There was a statistically significant difference between mean scute growth rates (in µm per y) of males (n=4) and females (n=6) (Welch's t-test, $t(8.9)=2.723$, $p=0.024$), with female scute keratin accumulating more slowly (69.06±51.70 µm per y) than males (131.78±24.40 µm per y). This difference is more pronounced when the mean model-predicted scute growth rate of female 13,326 is excluded from analysis as an outlier (Tukey's Fences, k=1.5), resulting in mean female scute growth rates of 51.06±22 µm per y. There was no statistically significant difference between loggerheads that stranded in the Gulf of Mexico (n=6) versus the Atlantic (n=6), ($t(8.8)=-0.147$, $p=0.886$).

Based on the model-predicted accumulation rates for green turtles (Fig. 3; Table 1), the mean time (±1 SD) required for the growth of 50 µm of scute keratin in the neritic individuals (n=6) was 0.65±0.16 y, and 1.13±0.34 y in oceanic individuals (n=3). All except one of the green turtles exhibited an overall decrease in scute growth rates

Fig. 3 Intra-individual scute growth rates of female (**a**) and male (**b**) green turtles, and female (**c**) and male (**d**) loggerhead turtles. Shaded areas represent 95% credible intervals for the posterior keratin growth rate estimates for each turtle

Table 1 Mean growth rates for green turtle and loggerhead turtle scute as calculated using modelled ^{14}C data

Species	ID	Sex	SCL (cm)	Life stage	Collection region	Scute thickness (µm)	Mean growth rate (µm per year)	SD (µm per year)	Mean growth rate (years per 50 µm)
Green	13588	M	30.2	Oceanic	SAB	450	37.5	6.2	1.33
Green	13590	M	91	Neritic	SAB	400	75.2	22.6	0.67
Green	13765	F	103.2	Neritic	SAB	300	60.8	25.0	0.82
Green	13769	F	37	Oceanic	SAB	250	38.0	3.3	1.32
Green	13776*	F	36.2	Oceanic	SAB	350	67.5	14.1	0.74
Green	13796	F	90.6	Neritic	SNWA	500	75.9	24.5	0.66
Green	13983	M	95	Neritic	SNWA	300	60.1	21.7	0.83
Green	13987	F	77	Neritic	EGOM	550	122.0	56.5	0.41
Green	13994	M	102.9	Neritic	SAB	350	92.6	46.6	0.54
Loggerhead	12954	F	74	Neritic	SAB	200	40.7	4.5	1.23
Loggerhead	13326	F	92.5	Neritic	SAB	500	177.1	48.4	0.28
Loggerhead	13328	M	102.1	Neritic	SAB	850	157.6	75.6	0.32
Loggerhead	*13587*	*F*	*82.3*	*Neritic*	*SAB*	*400*	*191.4*	*98.6*	*0.26*
Loggerhead	13771	F	84	Neritic	SAB	250	26.4	10.3	1.89
Loggerhead	13982	M	85.5	Neritic	SAB	400	106.3	50.7	0.47
Loggerhead	13992	F	88.9	Neritic	SAB	300	56.2	24.4	0.89
Loggerhead	12951	F	84.3	Neritic	NGOM	300	61.4	14.5	0.81
Loggerhead	12956	M	63.6	Neritic	NGOM	700	116.3	56.3	0.43
Loggerhead	12957	F	91.6	Neritic	NGOM	250	34.6	13.3	1.45
Loggerhead	*13324*	*F*	*82.7*	*Neritic*	*NGOM*	*800*	*691.6*	*32.2*	*0.07*
Loggerhead	13327	F	71.4	Neritic	NGOM	400	87.0	44.7	0.57
Loggerhead	*13764*	*F*	*97.9*	*Neritic*	*EGOM*	*400*	*18.4*	*18.0*	*2.72*
Loggerhead	12952	M	76.7	Neritic	EGOM	650	449.0	6.8	0.11
Loggerhead	12953	M	69	Neritic	EGOM	800	147.0	22.5	0.34

Collection regions are as follows: SAB = South Atlantic Bight, SNWA = Subtropical Northwest Atlantic, EGOM = Eastern Gulf of Mexico, NGOM = Northern Gulf of Mexico. Samples in italics returned values lower than the coral-otolith reference curve and were excluded from further statistical analysis because they could not be reliably modelled. *Calibrated using the Bomb21NH2 curve (Hua et al. 2021). SCL = straight carapace length

through time. Although there was no statistically significant difference between scute growth rates (in µm per y) of oceanic ($n=3$) versus neritic individuals ($n=6$), ($t(5.5)=2.432$, $p=0.055$), the oceanic individuals exhibited slower scute growth rates on average (47.7 ± 17.20 µm per y) than the neritic individuals (81.1 ± 23.30 µm per y). There was no statistically significant difference in the scute growth rates between neritic female ($n=3$) and male ($n=3$) green turtles, ($t(3)=-0.500$, $p=0.653$).

There was no statistically significant difference between the model-predicted mean scute growth rates (in µm per y) of the neritic green ($n=6$) and loggerhead ($n=11$) turtles ($t(14.7)=0.581$, $p=0.570$), nor was there a statistically significant difference in scute growth rate variability between neritic green and loggerhead turtles ($t(14.8)=0.681$, $p=0.506$).

Changepoint analysis of model-predicted scute growth rates

We applied changepoint analysis to the model-predicted scute growth rates of both loggerhead and green turtles to assess the synchronicity of the declining growth rates observed in several individuals across both species. Changepoint analysis revealed 2015–2016 and 2017–2018 as peak periods of declining scute growth rates, exhibiting the most frequent inflection points across 20 individuals (Fig. 4a). One green turtle (Turtle 13796) and three loggerhead turtles (Turtles 12953, 13326 and 13328) exhibited major declines in scute growth rates in 2015, whilst five green turtles (Turtles 13590, 13765, 13983, 13987 and 13994) and two loggerhead turtles (Turtles 13982 and 13992) exhibited similar declines in 2017–2018. Sensitivity testing demonstrates this is not likely an artefact of the ^{14}C calibration curve applied, as a different curve selection yields comparable results (see S1 and Figs. S28-S34). Changepoint analysis also detected peak periods of increasing growth rates (evident in Fig. 3 as a slowing of the rate of decrease) approximately six to

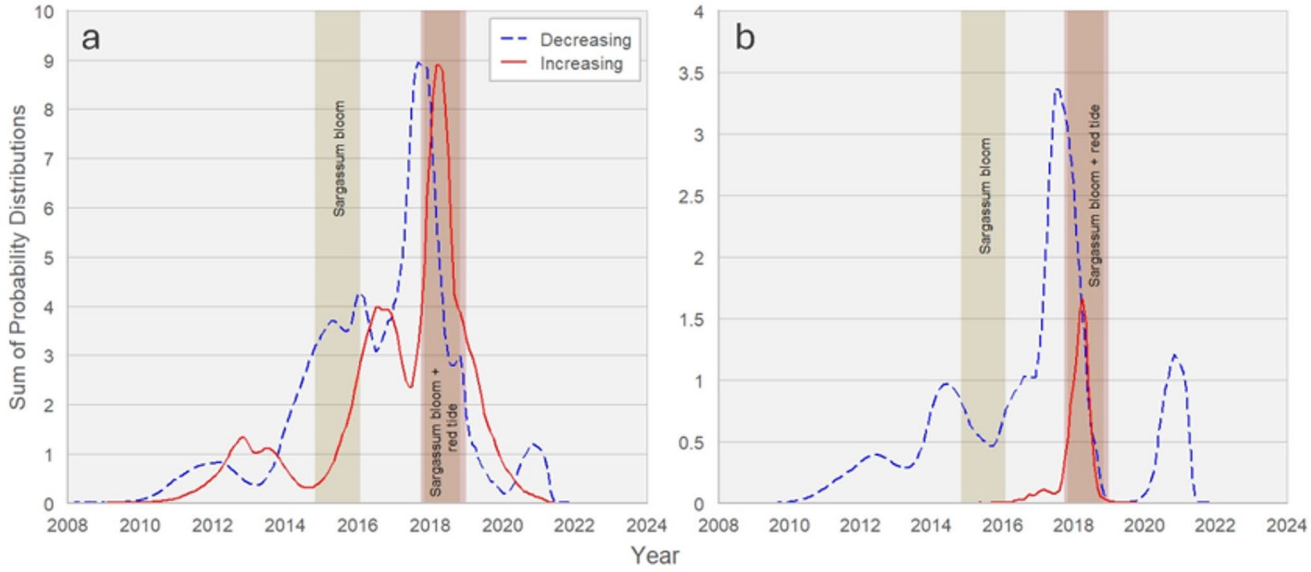

Fig. 4 Summed PDFs (probability density functions) representing (**a**) the occurrence of major changes across all analyzed turtles. Increasing changepoints (red, solid; $n = 20$) indicate an inflection towards higher growth rates. Decreasing changepoints (blue, dashed; $n = 25$) indicate the opposite, wherein a turtle has transitioned towards decreasing growth rates. (**b**) Summed PDFs of major reversal changepoints across all analyzed turtles. Increasing (red, solid; $n = 1$) and decreasing (blue; $n = 8$) lines denote changepoint distributions in turtles that represent a shift from decreasing rates to increasing rates or vice versa, indicating a major change in the growth response of the turtle

nine months after the peak years of decreasing growth rates (Fig. 4).

Discussion

Sequential $\Delta^{14}C$ analysis

In most individuals, the unmodelled sequential scute $\Delta^{14}C$ values followed the expected decline with increasing scute depth overall. However, in many instances, one or more keratin layers exhibited $\Delta^{14}C$ values that were lower than the subsequent layer (Supporting Information, Figs. S2 and S3). Given some of these reversals exceeded 15‰—beyond typical analytical uncertainty (±2‰)—they are unlikely to result from measurement error and suggest other influences. Two explanations are plausible: first, the introduction of exogenous carbon contamination to certain layers during sampling or processing, and secondly, the incorporation of ^{14}C-depleted dietary carbon by the turtles during keratin synthesis.

Although contamination from the adhesive used to affix the biopsies to the glass slides for sub-sampling cannot be excluded as a possibility, the age-depth relationships observed in our scute biopsies are inconsistent with contamination as a primary cause of the $\Delta^{14}C$ deviations. If the adhesive had partly percolated through the biopsies during sampling, we would expect a predictable and consistent age gradient – the keratin closest to the glass slide should appear oldest, with ages becoming progressively younger with distance. In all individuals except Turtle 13764 (discussed below), we do not observe this pattern. Random or sporadic inclusion of small amounts of adhesive into interior layers is possible, but given our rigorous cleaning protocol, contamination is unlikely to produce the significant offsets observed.

With these considerations in mind, we consider biological processes to be a more plausible explanation. Deviations from the expected monotonic decline in age with increasing scute depth could occur if turtles occasionally ingested resources that *(a)* contained inbuilt age, such as long-lived sponges, and/or *(b)* derived some of their dietary carbon from foraging areas affected by oil seeps or spills (Walker et al. 2017), upwelling (Toth et al. 2017), or estuarine waters (Andrews et al. 2020). Considering their migratory nature, it is plausible that turtles may have occasionally foraged in habitats beyond those represented by the coral-otolith calibration curve, incorporating dietary ^{14}C that is depleted or enriched relative to the local baseline due to the inherent spatial variation in ocean ^{14}C mixing.

One of the oceanic green turtles (Turtle 13776) exhibited unmodelled scute $\Delta^{14}C$ values that were lower than the coral-otolith reference series. During the oceanic stage, juvenile turtles subsist at the surface amongst floating offshore *Sargassum* mats, which form the base of the food web (Howell et al. 2016). Since *Sargassum* absorbs dissolved CO_2 from surface waters that are in equilibrium with the atmosphere, communities living within and upon the mats will primarily

reflect atmospheric ^{14}C concentrations. Because the carapace length of Turtle 13776 is consistent with the size at which green turtles recruit from oceanic to neritic habitats (Bjorndal et al. 2003), we theorized that the low $\Delta^{14}C$ values recorded within the scute layers were derived from atmospheric sources consumed prior to recruitment, and as such modelled the data using the atmospheric Bomb21NH2 curve (Hua et al. 2021).

Three of the neritic loggerheads (Turtles 13324, 13587 and 13764) also exhibited $\Delta^{14}C$ values across scute layers that were lower than the coral-otolith calibration curve but, given that their straight carapace lengths exceeded sizes observed in oceanic habitats (Bjorndal et al. 2000; Avens et al. 2013), it is unlikely they foraged within *Sargassum*-based food webs during recent scute growth. Instead, they may have consistently ingested ^{14}C-depleted resources at the time of keratin formation. Foraging in nearshore habitats influenced by the discharge of ^{14}C-depleted estuarine waters could feasibly result in the level of depletion observed in their scute biopsies. Indeed, discharge from Upper Floridian aquifer waters has been observed to decrease the $\Delta^{14}C$ values of grey snapper (*Lutjanus griseus*) otoliths in the Gulf of Mexico (Andrews et al. 2020), suggesting the dissolved inorganic carbon (DIC) in some nearshore locations is derived from a mixture of marine water and ^{14}C-depleted freshwater. If these turtles foraged consistently in areas with freshwater input, we might expect to see artificially old or artificially young ages in their scute biopsies depending on the extent of the freshwater ^{14}C input to the local marine DIC. Such low scute $\Delta^{14}C$ values might also result from the consumption of resources deriving carbon from areas affected by oil seeps and upwelling (Toth et al. 2017; Walker et al. 2017). Contamination of the biopsies by the adhesive cannot be ruled out and may be a more plausible explanation for Turtle 13764, whose unmodelled ^{14}C dates exhibit an age gradient opposite to the expected monotonic decline in age with scute depth.

Our inclusion of an r-type Outlier Model (Bronk Ramsey 2009b) in our Bayesian depositional models explicitly accounts for these offsets regardless of whether such deviations arise from minor contamination or dietary effects, downweighing measurements that deviate substantially from the expected stratigraphic relationship (see Figs. S4-S37).

Scute growth rates

The Bayesian chronological modelling approach both improves precision and provides insights into scute growth rate variability within individuals over time. Our results suggest the keratin growth rates of loggerhead and green turtles can vary over the life of an individual and between individuals.

The mean model-predicted loggerhead scute growth rate of 0.79 ± 0.53 y per 50 µm is slightly slower than the previous estimate of 0.6 y per 50 µm made on the basis of carbon turnover in juvenile loggerheads scaled to adult body size (Vander Zanden et al. 2010), and in neritic green turtles, the mean model-predicted scute growth rate of 0.65 ± 0.16 y per 50 µm is also slightly slower than the original estimate of 0.41 y per 50 µm in neritic adults (Vander Zanden et al. 2013).

Given the small sample size ($n = 11$), further work is required to establish whether the statistically significant slower scute growth rates in female loggerheads compared to male loggerheads is representative of wider populations. Slower female scute growth rates may be related to energetic trade-offs associated with vitellogenesis and nesting behaviors, whereby keratin accumulation and other maintenance processes are inhibited due to the high energetic requirements of reproductive processes (Pontzer and McGrosky 2022). Keratin growth rates have been observed to fall during reproductive cycles in several bird species, such as the barn swallow (*Hirundo rustica*) (Saino et al. 2014) and pied flycatcher (*Ficedula hypoleuca*) (Hemborg and Lundberg 1998), but to date no such studies have been carried out for chelonids. However, we might expect to see cyclical reductions in female scute growth rates that coincide with nesting seasons if metabolic trade-offs are the underlying cause of slower female scute growth rates, contrary to the observed temporal patterns in the female loggerheads analyzed in this study.

Our model-predicted mean growth rate of 1.13 ± 0.34 y per 50 µm for oceanic green turtles is considerably slower than the original estimate of 0.20 y per 50 µm (Vander Zanden et al. 2013) and, although there is no statistically significant difference, the scute growth rates of oceanic green turtles are slower than the neritic green turtles in this study (0.65 ± 0.16 y per 50 µm). The latter may be due to differences in prey and forage quality between habitats. Green turtles are mostly carnivorous during the oceanic stage, and prey availability in oceanic *Sargassum* habitats can be highly unpredictable compared to neritic habitats (Bjorndal et al. 2003; Roark et al. 2009). Juvenile green turtle somatic growth rates can therefore decrease during the oceanic stage in response to nutritional stress and increase during periods of compensatory growth (CG) when food availability improves in neritic habitats (Roark et al. 2009). Reductions in somatic growth rates are likely to result in reduced keratin accumulation. Alternatively, slower scute growth rates in juveniles may be due to the allocation of greater resources to overall somatic growth and development, much like certain passerine species who prioritize nestling growth and

the building of body mass over plumage development until after fledging (Kiat and Izhaki 2016).

Synchronized declines in scute growth rates

Changepoint analysis detected rapid decreases in scute growth rate occurring simultaneously during 2017–2018 in five green turtles (Turtles 13590, 13765, 13983, 13987 and 13994) and two loggerheads (Turtles 13982 and 13992) (Figs. 3 and 4), all followed by reductions in the rate of decline (categorized as 'Increasing' in Fig. 4). Considering that scute growth rates declined simultaneously in these individuals around the same calendar year, this may represent a widespread physiological response to an environmental or climatic event. Synchronous declines in somatic growth rates in response to factors such as ecological regime shifts and reduction in habitat quality have been previously observed in loggerhead, green and hawksbill turtle populations (Bjorndal et al. 2017; Kubis et al. 2009). Likewise, reductions in the growth rates of keratinized tissues have been observed in other species under reduced nutritional regimes, including Caspian terns (*Hydroprogne caspia*) (Patterson et al. 2015), domestic sheep (*Ovis aries*) (Schlink et al. 1998) and Alpine ibex (*Capra ibex*), which have also been documented to undergo synchronized inter-individual changes in horn keratin growth rates in response to environmental conditions (Büntgen et al. 2014).

One possible cause for the synchronous decline in scute growth rates observed here is the major 'red tide' event that occurred in the eastern Gulf of Mexico and along the east coast of Florida between September 2017 and January 2019, which is considered to have been the most intense harmful algal bloom (HAB) in the region since 2005 (Weisberg et al. 2019). These events are characterized by large, nearshore blooms of the harmful dinoflagellate *Karenia brevis*, which produce neurotoxins capable of killing invertebrates, fish, turtles and marine mammals (Hoagland et al. 2020) and can cause significant declines in seagrass cover due to the associated light attenuation (Kim et al. 2015). Unlike previous years where the onset of blooms occurred during late summer and subsequently diminished in the winter, cell counts during the 2018 event remained high for more than 12 months (Weisberg et al. 2019). In marine turtles, the neurological symptoms of mild exposure to these brevetoxins include loss of coordination, inability to submerge, and muscle twitching, whilst more severe exposure may cause lethargy and paralysis (Fauquier et al. 2013), which in turn may result in drowning and death (Perrault et al. 2021). All of these symptoms are capable of inhibiting foraging ability, with affected turtles submitted to rehabilitation facilities observed to be malnourished, hypoglycemic, and dehydrated (Perrault et al. 2021). The primary route of brevetoxin exposure is likely to be through the diet and the ingestion of sea water, whereby bioaccumulation in common forage and prey items such crustaceans can result in high concentrations of toxins being passed along the food chain to omnivorous marine turtle species like loggerheads (Nederlof et al. 2024). In seagrasses, brevetoxins have been shown to persist for up to eight months after a bloom has diminished, providing a constant source of exposure for primarily herbivorous species such as green turtles (Nederlof et al. 2024). Reductions in scute growth rates during the 2017–2019 red tide event may therefore be *(a)* a physiological effect of sublethal brevetoxin accumulation, which has been correlated with decreased body condition, oxidative stress, and increased tumor growth (Perrault et al. 2017), and/or *(b)* an effect of nutritional stress following reduced food availability and restricted ability to forage (Kim et al. 2015).

Alongside the 2017–2019 red tide event, an unprecedented Atlantic *Sargassum* bloom carried more than 20 million tonnes of wet biomass into the Gulf of Mexico in June 2018 (Wang et al. 2019). Massive accumulations of *Sargassum* along the foreshore can severely degrade coastal habitats by altering water chemistry, blocking light and creating physical barriers that impede the movements of larger marine species such as manatees and turtles (Louime et al. 2017; Van Tussenbroek et al. 2017). The decomposition of these mats creates hypoxic conditions and high concentrations of ammonium and hydrogen sulfide, which in 2018 resulted in the mass mortality of 78 species along the Mexican Caribbean coast (Rodríguez-Martínez et al. 2019). The second largest *Sargassum* bloom in recent years impacted the region a few years prior in 2015, with over nine million tonnes of wet biomass (Wang et al. 2019). Given that three other loggerheads (Turtles 12953, 13326 and 13328) and one other green turtle (Turtle 13796) also exhibited drastic reductions in their model-predicted scute growth rates around 2015 and are further detected through changepoint analysis (Fig. 4), the widespread environmental impacts of these two *Sargassum* blooms are another plausible explanation for the reduction of scute growth rates seen in green and loggerhead turtles in 2015 and 2018. A reduction in the availability of seagrass and prey items combined with impeded mobility caused by a combination of *Sargassum* accumulation and the neurological impacts of brevetoxin exposure may have resulted in reduced nutrient intake and higher stress among turtle populations foraging in affected areas, thereby reducing scute growth rates.

A persistent pattern across the changepoint distributions is the presence of 'increasing' changes in scute growth rates approximately six to nine months after the synchronous decreases observed around 2015 and 2018, which may represent a slight alleviation of poor conditions (Fig. 4A).

Only a single turtle exhibits an increasing growth change immediately following the 2018 decline (Fig. 4B). The rest of the 'increasing' changes that lag the sharp declines in growth during 2015 and 2018 instead indicate a cessation in declining rates, with a transition to stable periods at lower growth rates (Fig. 3). None of the turtles that exhibited the synchronous decline returned to their original scute growth rates prior to stranding and death, suggesting that if these events are indeed the cause of the decline, the physiological impacts of HABs or macroalgal blooms on green and loggerhead turtles may be long-lasting. This pattern is consistent with long-term studies of the effects of HABs on benthic communities, with recovery estimates ranging from 3 to 5 years (Kröger et al. 2006; Turner et al. 2021). Under continued physiological and nutritional stress, reproductive function (and therefore population density) in reptiles can be impacted (Greenberg and Wingfield 1987; Moore and Jessop 2003). Given that the severity, frequency, extent and duration of harmful algal blooms and *Sargassum* inundations is increasing both in Florida and globally (Wang et al. 2019; Heil and Muni-Morgan 2021) due to anthropogenic activity and climate change (Walsh et al. 2006; Lapointe et al. 2015; Gobler 2020), understanding their impacts on marine turtle populations is therefore critical to conservation efforts.

Our results provide new insights into the growth dynamics of loggerhead and green turtle scutes, offering a chronological framework for the reconstruction of trophic ecology, ontogenetic shifts, and habitat use from sequential stable isotope data. Beyond marine turtles, this approach holds broad applicability for other incrementally formed, isotopically informative tissues—such as baleen in endangered whales or hair in migratory terrestrial animals—opening new opportunities to explore individual life histories in fine temporal detail. Importantly, the identification of synchronous shifts in growth rates also illustrates the potential for this method to detect widespread physiological responses to environmental change, shedding light on the lasting impacts of ecological disturbances.

Supplementary Information The online version contains supplementary material available at https://doi.org/10.1007/s00227-025-04792-4.

Acknowledgements We extend our sincere gratitude to Karrie Minch and the Sea Turtle Stranding and Salvage Network (STSSN) for their generous support in allowing us to attend and collect samples during their organized necropsy sessions. Additionally, we sincerely thank Christopher Nolte and Kate Davis for their dedicated assistance during tissue collection. We are especially grateful to Dr. Brian Stacy (NOAA) for his invaluable assistance with sampling efforts during the COVID-19 closures. We greatly appreciate the comments of two anonymous reviewers which enhanced the manuscript.

Author contributions All authors contributed to the study conception and design. Material preparation and data collection were performed by Amy A. Wallace, Alexandra L. Fireman and Jenna D. Bennett. Data analysis was performed by Bethan Linscott, Lorena Becerra-Valdivia and Matt R. P. Harris. The first draft of the manuscript was written by Bethan Linscott, and all authors commented on previous versions of the manuscript. All authors read and approved the final manuscript.

Funding This work was funded in part by the Florida RESTORE Act Centers of Excellence Research Grants Program, Subagreement No. 4710-1129-00-B awarded to Hannah Vander Zanden and Will Patterson III.

Data availability Radiocarbon data associated with this publication are available at the Gulf Science Data Repository, GRIID-C. For scute radiocarbon measurements, see 'Sequential bomb radiocarbon data for scute growth rate estimation in green (*Chelonia mydas*) and loggerhead (*Caretta caretta*) sea turtles' (https://data.griidc.org/data/F3.x304.000:0004; https://doi.org/10.7266/wf62nacr). For the coral-otolith reference series, see 'Gulf of Mexico coral and otolith radiocarbon curve' (https://data.griidc.org/data/F3.x304.000:0002; https://doi.org/10.7266/5vsz0kfh). All code used to perform the changepoint analysis and associated data preparation is available at https://github.com/MRPHarris/TurtleScuteCPTs. All other data are available in the main text or the Supporting Information.

Declarations

Competing interests Authors declare that they have no competing interests.

Ethics approval All turtle scute collections and tissue dissections were carried out under Marine Turtle Permits MTP-20-016, MTP-21-016, and MTP-22-016 granted by Florida Fish and Wildlife Conservation Commission, and the University of Florida Institutional Animal Care and Use Committee (IACUC) protocol number 202001985.

References

Andrews AH, Kalish JM, Newman SJ, Johnston JM (2011) Bomb radiocarbon dating of three important reef-fish species using indo-pacific $\Delta^{14}C$ chronologies. Mar Freshwater Res 62(11):1259–1269

Andrews AH, Barnett BK, Chanton JP, Thornton LA, Allman RJ (2020) Influences of upper Floridan aquifer waters on radiocarbon in the otoliths of Gray snapper (*Lutjanus griseus*) in the Gulf of Mexico. Radiocarbon 62(5):1127–1146

Avens L, Goshe LR, Pajuelo M, Bjorndal KA, MacDonald BD, Lemons GE, Bolten AB, Seminoff JA (2013) Complementary skeletochronology and stable isotope analyses offer new insight into

juvenile loggerhead sea turtle oceanic stage duration and growth dynamics. Mar Ecol Prog Ser 491:235–251

Barnett BK, Thornton L, Allman R, Chanton JP, Patterson WF III (2018) Linear decline in red snapper (*Lutjanus campechanus*) otolith $\Delta^{14}C$ extends the utility of the bomb radiocarbon chronometer for fish age validation in the northern Gulf of Mexico. ICES J Mar Sci 75(5):1664–1671

Barnett BK, Chanton JP, Ahrens R, Thornton L, Patterson WF III (2020) Life history of northern Gulf of Mexico warsaw grouper *Hyporthodus nigritus* inferred from otolith radiocarbon analysis. PLoS One 15(1):e0228254

Bjorndal KA, Bolten AB, Martins HR (2000) Somatic growth model of juvenile loggerhead sea turtles *Caretta caretta*: duration of pelagic stage. Mar Ecol Prog Ser 202:265–272

Bjorndal KA, Bolten AB, Dellinger T, Delgado C, Martins HR (2003) Compensatory growth in oceanic loggerhead sea turtles: response to a stochastic environment. Ecology 84(5):1237–1249

Bjorndal KA, Bolten AB, Chaloupka M, Saba VS, Bellini C, Marcovaldi MA, Santos AJ, Bortolon LFW, Meylan AB, Meylan PA (2017) Ecological regime shift drives declining growth rates of sea turtles throughout the West Atlantic. Glob Chang Biol 23(11):4556–4568

Bolten AB (2003) Active swimmers – passive drifters: The oceanic juvenile stage of loggerheads in the Atlantic system. In: Bolten AB (ed) Loggerhead Sea Turtles. Smithsonian Institution Press, Washington DC, pp 63–78

Bolten AB, Lutz PL, Musick JA, Wyneken J (2003) Variation in sea turtle life history patterns: Neritic vs oceanic developmental stages. In: Lutz PL, Musick JA, Wyneken J (eds) The Biology of Sea Turtles Vol II. CRC Press, pp 243–257

Bolten B, Crowder LB, Dodd MG, Lauritsen AM, Musick JA, Schroeder BA, Witherington BE (2019) Recovery plan for the Northwest Atlantic population of the loggerhead sea turtle (*Caretta caretta*). Second revision (2008). Assessment of Progress Toward Recovery. 21 p

Bronk Ramsey C (2008a) Radiocarbon dating: revolutions in understanding. Archaeometry 50:249–275

Bronk Ramsey C (2008b) Deposition models for chronological records. Quat Sci Rev 27(1–2):42–60

Bronk Ramsey C (2009a) Bayesian analysis of radiocarbon dates. Radiocarbon 51(1):337–360

Bronk Ramsey C (2009b) Dealing with outliers and offsets in radiocarbon dating. Radiocarbon 51(3):1023–1045

Büntgen U, Liebhold A, Jenny H, Mysterud A, Egli S, Nievergelt D, Stenseth NC, Bollmann K (2014) European springtime temperature synchronises ibex horn growth across the Eastern Swiss alps. Ecol Lett 17(3):303–313

Cadd H, Petherick L, Tyler J, Herbert A, Cohen TJ, Sniderman K, Barrows TT, Fulop RH, Knight J, Kershaw AP (2021) A continental perspective on the timing of environmental change during the last glacial stage in Australia. Quat Res 102:5–23

Cerling TE, Wittemyer G, Ehleringer JR, Remien CH, Douglas-Hamilton I (2009) History of animals using isotope records (HAIR): a 6-year dietary history of one family of African elephants. PNAS 106(20):8093–8100

Chamberlin DW, Siders ZA, Barnett BK, Ahrens RN, Patterson WF III (2023) Highly variable length-at-age in vermilion snapper (*Rhomboplites aurorubens*) validated via Bayesian analysis of bomb radiocarbon. Fish Res 264:106732

Doubleday ZA, Hosking L, Willoughby J, Dias M, Leclerc N, Nikolajew SB, Peharda M, Rézio AT, Trueman C (2025) Capitalizing on the wealth of chemical data in the accretionary structures of aquatic taxa: opportunities from across the tree of life. Limnol Oceanogr Lett 10(1):18–36

Druffel EM (1980) Radiocarbon in annual coral rings of Belize and Florida. Radiocarbon 22(2):363–371

Druffel ER (1989) Decade time scale variability of ventilation in the North Atlantic: high-precision measurements of bomb radiocarbon in banded corals. J Geophys Res Oceans 94(C3):3271–3285

Druffel ER, Griffin S (1993) Large variations of surface ocean radiocarbon: evidence of circulation changes in the Southwestern Pacific. J Geophys Res Oceans 98(C11):20249–20259

Druffel EM, Linick TW (1978) Radiocarbon in annual coral rings of Florida. Geophys Res Lett 5(11):913–916

Ehrlén J, Morris WF (2015) Predicting changes in the distribution and abundance of species under environmental change. Ecol Lett 18(3):303–314

Fauquier DA, Flewelling LJ, Maucher J, Manire CA, Socha V, Kinsel MJ, Stacy BA, Henry M, Gannon J, Ramsdell JS (2013) Brevetoxin in blood, biological fluids, and tissues of sea turtles naturally exposed to *Karenia brevis* blooms in central West Florida. J Zoo Wildl Med 44(2):364–375

Figgener C, Bernardo J, Plotkin PT (2019) Beyond trophic morphology: stable isotopes reveal ubiquitous versatility in marine turtle trophic ecology. Biol Rev 94(6):1947–1973

Fireman AL, Stapleton SP, Vander Zanden HB, Liang D, Woodland RJ (2024) Ecological niche use varies with sea turtle reproductive age. Mar Biol 171(11):214

Gobler CJ (2020) Climate change and harmful algal blooms: insights and perspective. Harmful Algae 91:101731

Greenberg N, Wingfield JC (1987) Stress and reproduction: Reciprocal relationships. In: Norris DO, Jones RE (eds) Hormones and Reproduction in Fishes, Amphibians and Reptiles. Springer, pp 461–503

Hajdas I (2008) Radiocarbon dating and its applications in quaternary studies. EGQSJ 57(1/2):2–24

Hajdas I, Ascough P, Garnett MH, Fallon SJ, Pearson CL, Quarta G, Spalding KL, Yamaguchi H, Yoneda M (2021) Radiocarbon dating. Nat Rev Methods Primers 1(1):62

Haywood JC, Fuller WJ, Godley BJ, Shutler JD, Widdicombe S, Broderick AC (2019) Global review and inventory: how stable isotopes are helping us understand ecology and inform conservation of marine turtles. Mar Ecol Prog Ser 613:217–245

Heil CA, Muni-Morgan AL (2021) Florida's harmful algal bloom (HAB) problem: escalating risks to human, environmental and economic health with climate change. Front Ecol Evol 9:646080

Hemborg C, Lundberg A (1998) Costs of overlapping reproduction and moult in passerine birds: an experiment with the pied flycatcher. Behav Ecol Sociobiol 43:19–23

Hoagland P, Kirkpatrick B, Jin D, Kirkpatrick G, Fleming LE, Ullmann SG, Beet A, Hitchcock G, Harrison KK, Li ZC, Bruce G, Diaz RE, Vince L (2020) Lessening the hazards of Florida red tides: a common sense approach. Front Mar Sci 7:538

Howell LN, Reich KJ, Shaver DJ, Landry AM Jr, Gorga CC (2016) Ontogenetic shifts in diet and habitat of juvenile green sea turtles in the northwestern Gulf of Mexico. Mar Ecol Prog Ser 559:217–229

Hua Q, Turnbull JC, Santos GM, Rakowski AZ, Ancapichún S, De Pol-Holz R, Hammer S, Lehman SJ, Levin I, Miller JB (2021) Atmospheric radiocarbon for the period 1950–2019. Radiocarbon 64(4):723–745

Kalish JM (1993) Pre- and post-bomb radiocarbon in fish otoliths. Earth Planet Sci Lett 114(4):549–554

Kastelle CR, Kimura DK, Goetz BJ (2008) Bomb radiocarbon age validation of Pacific Ocean perch (*Sebastes alutus*) using new statistical methods. Can J Fish Aquat Sci 65(6):1101–1112

Katzenberg MA, Waters-Rist AL (2018) Stable isotope analysis: A tool for studying past diet demography and life history. In: Katzenberg MA, Saunders SR (eds) Biological Anthropology of the Human Skeleton. Wiley-Blackwell, pp 467–504

Kiat Y, Izhaki I (2016) Why renew fresh feathers? Advantages and conditions for the evolution of complete post-juvenile moult. J Avian Biol 47(1):47–56

Killick R, Eckley IA (2014) Changepoint: an R package for changepoint analysis. J Stat Softw 58:1–19

Kim YK, Kim SH, Lee KS (2015) Seasonal growth responses of the seagrass *Zostera marina* under severely diminished light conditions. Estuaries Coasts 38:558–568

Kröger K, Gardner JP, Rowden AA, Wear RG (2006) Long-term effects of a toxic algal bloom on subtidal soft-sediment macroinvertebrate communities in Wellington harbour new Zealand. Estuar Coast Shelf Sci 67(4):589–604

Kubis S, Chaloupka M, Ehrhart L, Bresette M (2009) Growth rates of juvenile green turtles *Chelonia mydas* from three ecologically distinct foraging habitats along the East central Coast of Florida USA. Mar Ecol Prog Ser 389:257–269

Lapointe BE, Herren LW, Debortoli DD, Vogel MA (2015) Evidence of sewage-driven eutrophication and harmful algal blooms in Florida's Indian River Lagoon. Harmful Algae 43:82–102

Linscott B, Pike AW, Angelucci DE, Cooper MJ, Milton JS, Matias H, Zilhão J (2023) Reconstructing Middle and Upper Paleolithic human mobility in Portuguese Estremadura through laser ablation strontium isotope analysis. PNAS 120(20):p.e2204501120

López-Castro MC, Bjorndal KA, Bolten AB (2014) Evaluation of scute thickness to infer life history records in the carapace of green and loggerhead turtles. Endanger Species Res 24(3):191–196

Louime C, Fortune J, Gervais G (2017) *Sargassum* invasion of coastal environments: a growing concern. Am J Environ Sci 13(1):58–64

Moore IT, Jessop TS (2003) Stress reproduction and adrenocortical modulation in amphibians and reptiles. Horm Behav 43(1):39–47

Moyer R, Grottoli A (2011) Coral skeletal carbon isotopes ($\delta^{13}C$ and $\Delta^{14}C$) record the delivery of terrestrial carbon to the coastal waters of Puerto Rico. Coral Reefs 30:791–802

Nederlof RA, van der Veen D, Perrault JR, Bast R, Barron HW, Bakker J (2024) Emerging insights into brevetoxicosis in sea turtles. Animals 14(7):991

Patterson AG, Kitaysky AS, Lyons DE, Roby DD (2015) Nutritional stress affects corticosterone deposition in feathers of Caspian Tern chicks. J Avian Biol 46(1):18–24

Pearson RM, van de Merwe JP, Limpus CJ, Connolly RM (2017) Realignment of sea turtle isotope studies needed to match conservation priorities. Mar Ecol Prog Ser 583:259–271

Perrault JR, Stacy NI, Lehner AF, Mott CR, Hirsch S, Gorham JC, Buchweitz JP, Bresette MJ, Walsh CJ (2017) Potential effects of brevetoxins and toxic elements on various health variables in kemp's ridley (*Lepidochelys kempii*) and green (*Chelonia mydas*) sea turtles after a red tide bloom event. Sci Total Environ 605:967–979

Perrault JR, Barron HW, Malinowski CR, Milton SL, Manire CA (2021) Use of intravenous lipid emulsion therapy as a novel treatment for brevetoxicosis in sea turtles. Sci Rep 1(1):24162

Pontzer H, McGrosky A (2022) Balancing growth reproduction maintenance and activity in evolved energy economies. Curr Biol 32(12):709–719

Reich KJ, Bjorndal KA, Bolten AB (2007) The 'lost years' of green turtles: using stable isotopes to study cryptic lifestages. Biol Lett 3(6):712–714

Reich KJ, Bjorndal KA, del Martínez Rio C (2008) Effects of growth and tissue type on the kinetics of $\delta^{13}C$ and $\delta^{15}N$ incorporation in a rapidly growing ectotherm. Oecologia 155:651–663

Roark AM, Bjorndal KA, Bolten AB (2009) Compensatory responses to food restriction in juvenile green turtles (*Chelonia mydas*). Ecology 90(9):2524–2534

Rodríguez-Martínez RE, Medina-Valmaseda AE, Blanchon P, Monroy-Velázquez L, Almazán-Becerril A, Delgado-Pech B, Vásquez-Yeomans L, Francisco V, García-Rivas M (2019) Faunal mortality associated with massive beaching and decomposition of pelagic sargassum. Mar Pollut Bull 146:201–205

Saino N, Romano M, Rubolini D, Ambrosini R, Romano A, Caprioli M, Costanzo A, Bazzi G (2014) A trade-off between reproduction and feather growth in the barn swallow (*Hirundo rustica*). PLOS ONE 9(5):e96428

Schlink A, Mata G, Lewis R (1998) Consequences of differing wool growth rates on staple strength of Merino wethers with divergent staple strengths. Wool Tech Sheep Breed 46(3):271–285

Seminoff JA, Philliott AD (2020) Stable isotope analyses of sea turtles a review of three recent global reviews and data assessments. Mar Ecol Prog Ser 583:259–271

Seminoff JA, Allen CD, Balazs GH, Dutton PH, Eguchi T, Haas H, Hargrove SA, Jensen M, Klemm DL, Lauritsen AM, MacPherson SL (2015) Status review of the green turtle (*Chelonia mydas*) under the Endangered Species Act. National Oceanic and Atmospheric Administration

Shimada T, Aoki S, Kameda K, Hazel J, Reich K, Kamezaki N (2014) Site fidelity ontogenetic shift and diet composition of green turtles (*Chelonia mydas*) in Japan inferred from stable isotope analysis. Endanger Species Res 25(2):151–164

Toth LT, Cheng H, Edwards RL, Ashe E, Richey JN (2017) Millennial-scale variability in the local radiocarbon reservoir age of South Florida during the holocene. Quat Geochronol 42:130–143

Trueman CN, Rickaby RE, Shephard S (2013) Thermal, trophic and metabolic life histories of inaccessible fishes revealed from stable-isotope analyses: a case study using orange roughy *Hoplostethus atlanticus*. J Fish Biol 2013;83(6):1613–36

Turner AD, Lewis AM, Bradley K, Maskrey BH (2021) Marine invertebrate interactions with harmful algal blooms–implications for one health. J Invertebr Pathol 186:107555

Van Houtan KS, Andrews AH, Jones TT, Murakawa SK, Hagemann ME (2016) Time in tortoiseshell a bomb radiocarbon-validated chronology in sea turtle scutes. Proc R Soc B Biol Sci 283(1822):20152220

Van Houtan KS, Jones TT, Hagemann ME, Schumacher J, Phocas G, Gaos AR, Seminoff JA (2023) Sequential scute growth layers reveal developmental histories of hawksbill sea turtles. Mar Biol 170(7):79

Van Tussenbroek BI, Arana HAH, Rodríguez-Martínez RE, Espinoza-Avalos J, Canizales-Flores HM, González-Godoy CE, Barba-Santos MG, Vega-Zepeda A, Collado-Vides L (2017) Severe impacts of brown tides caused by *Sargassum* spp. on near-shore Caribbean seagrass communities. Mar Pollut Bull 122(1–2):272–281

Vander Zanden HB, Bjorndal KA, Reich KJ, Bolten AB (2010) Individual specialists in a generalist population: results from a long-term stable isotope series. Biol Lett 6(5):711–714

Vander Zanden HB, Bjorndal KA, Bolten AB (2013) Temporal consistency and individual specialization in resource use by green turtles in successive life stages. Oecologia 173:767–777

Vander Zanden HB, Tucker AD, Hart KM, Lamont MM, Fujisaki I, Addison DS, Mansfield KL, Phillips KF, Wunder MB, Bowen GJ (2015) Determining origin in a migratory marine vertebrate: a novel method to integrate stable isotopes and satellite tracking. Ecol Appl 25(2):320–335

Wagner AJ (2009) Oxygen and carbon isotopes and coral growth in the Gulf of Mexico and Caribbean Sea as environmental and climate indicators. PhD Dissertation, Texas A&M University

Wagner AJ, Guilderson TP, Slowey NC, Cole JE (2009) Pre-bomb surface water radiocarbon of the Gulf of Mexico and Caribbean as recorded in hermatypic corals. Radiocarbon 51(3):947–954

Walker B, Druffel E, Kolasinski J, Roberts B, Xu X, Rosenheim B (2017) Stable and radiocarbon isotopic composition of dissolved organic matter in the Gulf of Mexico. Geophys Res Lett 44(16):8424–8434

Wallace AA, Hollander DJ, Peebles EB (2014) Stable isotopes in fish eye lenses as potential recorders of trophic and geographic history. PLOS One 9(10):e108935

Walsh JJ, Jolliff J, Darrow B, Lenes J, Milroy S, Remsen A, Dieterle D, Carder KL, Chen F, Vargo GA (2006) Red tides in the Gulf of Mexico: where, when, and why. J Geophys Res Oceans 111:C11003

Wang M, Hu C, Barnes BB, Mitchum G, Lapointe B, Montoya JP (2019) The great Atlantic sargassum belt. Science 365(6448):83–87

Weisberg RH, Liu Y, Lembke C, Hu C, Hubbard K, Garrett M (2019) The coastal ocean circulation influence on the 2018 west Florida shelf *K. brevis* red tide bloom. J Geophys Res Oceans 124(4):2501–2512